Bioactive Materials 35 (2024) 1–16

Contents lists available at ScienceDirect

Bioactive Materials

journal homepage: www.keaipublishing.com/en/journals/bioactive-materials

Heterogeneous DNA hydrogel loaded with Apt02 modified tetrahedral framework nucleic acid accelerated critical-size bone defect repair

Yafei Han [a,c,e,f,1], Yan Wu [a,c,1], Fuxiao Wang [a,c,e,f,1], Guangfeng Li [a,c,e,h,1], Jian Wang [a,c,e,f], Xiang Wu [a,c,e], Anfu Deng [a,c,e], Xiaoxiang Ren [a,c], Xiuhui Wang [a,c], Jie Gao [e,**], Zhongmin Shi [g,***], Long Bai [a,c,d,****], Jiacan Su [a,b,c,*]

[a] Organoid Research Center, Institute of Translational Medicine, Shanghai University, Shanghai, 200444, China
[b] Department of Orthopedics, Xinhua Hospital Affiliated to Shanghai Jiao Tong University School of Medicine, Shanghai, 200092, China
[c] National Center for Translational Medicine (Shanghai) SHU Branch, Shanghai University, Shanghai, 200444, China
[d] Wenzhou Institute of Shanghai University, Wenzhou, 325000, China
[e] School of Medicine, Shanghai University, Shanghai, 200444, China
[f] School of Environmental and Chemical Engineering, Shanghai University, Shanghai, 200444, China
[g] National Center for Orthopaedics, Shanghai Sixth People's Hospital, Shanghai, 200233, China
[h] Department of Orthopedics, Shanghai Zhongye Hospital, Shanghai, 200444, China

ARTICLE INFO

Keywords:
DNA hydrogel
tFNA
Aptamer02
Angiogenesis
Bone regeneration

ABSTRACT

Segmental bone defects, stemming from trauma, infection, and tumors, pose formidable clinical challenges. Traditional bone repair materials, such as autologous and allogeneic bone grafts, grapple with limitations including source scarcity and immune rejection risks. The advent of nucleic acid nanotechnology, particularly the use of DNA hydrogels in tissue engineering, presents a promising solution, attributed to their biocompatibility, biodegradability, and programmability. However, these hydrogels, typically hindered by high gelation temperatures (~46 °C) and high construction costs, limit cell encapsulation and broader application. Our research introduces a novel polymer-modified DNA hydrogel, developed using nucleic acid nanotechnology, which gels at a more biocompatible temperature of 37 °C and is cost-effective. This hydrogel then incorporates tetrahedral Framework Nucleic Acid (tFNA) to enhance osteogenic mineralization. Furthermore, considering the modifiability of tFNA, we modified its chains with Aptamer02 (Apt02), an aptamer known to foster angiogenesis. This dual approach significantly accelerates osteogenic differentiation in bone marrow stromal cells (BMSCs) and angiogenesis in human umbilical vein endothelial cells (HUVECs), with cell sequencing confirming their targeting efficacy, respectively. *In vivo* experiments in rats with critical-size cranial bone defects demonstrate their effectiveness in enhancing new bone formation. This innovation not only offers a viable solution for repairing segmental bone defects but also opens avenues for future advancements in bone organoids construction, marking a significant advancement in tissue engineering and regenerative medicine.

1. Introduction

The repair of various types of bone defects caused by severe diseases such as trauma, infections, and tumors, particularly large segmental defects in long bones, remains a significant challenge for orthopedic surgeons [1]. Autologous bone grafting, despite being a conventional treatment method with notable effectiveness, is limited by the availability of bone from the patient's body [2]. Allogeneic bone grafting, on the other hand, poses risks of immune rejection and disease transmission [3]. In recent years, the emergence of bone tissue engineering has

Peer review under responsibility of KeAi Communications Co., Ltd.
* Corresponding authors. Organoid Research Center, Institute of Translational Medicine, Shanghai University, Shanghai, 200444, China.
** Corresponding author.
*** Corresponding authors.
**** Corresponding author. Organoid Research Center, Institute of Translational Medicine, Shanghai University, Shanghai, 200444, China.
E-mail addresses: jmsx2021@shu.edu.cn (J. Gao), 18930177323@163.com (Z. Shi), bailong@shu.edu.cn (L. Bai), drsujiacan@163.com (J. Su).
[1] The four authors contributed equally to this work.

https://doi.org/10.1016/j.bioactmat.2024.01.009
Received 7 December 2023; Received in revised form 10 January 2024; Accepted 10 January 2024
Available online 18 January 2024

opened new research directions for the treatment of large segmental bone defects [4–9]. The integration of bone formation-related active factors with biologically active material scaffold carriers marks the beginning and the key in the construction of bone tissue engineering [10,11]. It also represents a current research hotspot.

Nucleic acid nanotechnology, leveraging DNA or RNA, is employed to construct various nanostructures (e.g., nanotube, origami, nanoflower, nanorobot) with predetermined designs [12]. Its extensive application in biomedical research spans biosensing, tissue regeneration, targeted drug delivery, and cancer therapy [13]. Among them, the use of DNA hydrogels in tissue engineering presents a promising solution, attributed to their biocompatibility biodegradability, and programmability [14,15]. Reported to enhance bone repair, the effectiveness of DNA hydrogels is attributed to their phosphate-rich backbone and adenine content, providing biocompatibility, editability, and structural controllability. However, their synthesis, requiring high oligonucleotide concentrations, is costly and they degrade rapidly. Additionally, the synthesis reaction temperature of DNA hydrogels, which is 46.3 °C [16], and has been traditionally used traditionally, is unsuitable for cell encapsulation. Thus, there is a dire need to develop a cost-effective new type of DNA hydrogel for bone repair. The DNA hydrogel designed in this study uses an acrylamide polymer as the main chain and DNA crosslinkers as side chains, forming a DNA polymer through base complementary pairing. The use of 64 different DNA single strands as crosslinkers allows for a uniform gel formation. Furthermore, the introduction of complementary short strands of the crosslinkers enables self-assembly at a more moderate temperature of 37 °C, suitable for cell encapsulation and significantly reducing the production cost of traditional DNA hydrogels. Subsequent tests using actin have shown that it greatly slow down its degradation, making it suitable for long-term bone repair applications. The unique editability of the DNA hydrogel allows for varying the number of crosslinkers to adjust its physical properties, enabling the creation of a hydrogel tailored to specific experimental purposes. However, considering the limited osteogenic capacity of DNA hydrogels, which are not effective in rapidly inducing new bone formation, there is an emerging focus on incorporating active components into DNA hydrogels to expedite bone formation.

tFNA, another DNA nanostructure characterized by its framework shape and self-assembled from four specific single-stranded DNAs, holds certain advantages in the field of tissue engineering [17]. Its potential in inducing stem cells towards osteogenic differentiation, promoting vascular regeneration, neural modulation, and immune regulation makes it a promising candidate for bone regeneration [18,19]. The introduction of tFNA into DNA hydrogel is expected to significantly enhance the active mineralization capability of the DNA hydrogel, accelerating new bone matrix formation and deposition. Bone repair is often accompanied by angiogenesis, where rapid vascularization can effectively promote bone formation [20–22]. Therefore, the addition of active molecules that stimulate angiogenesis can enhance neovascularization and thereby facilitate bone regeneration. Apt02 is a DNA aptamer with Vascular Endothelial Growth Factor A (VEGFA) mimetic activity, capable of binding to vascular endothelial growth factor receptors VEGFR-1 and VEGFR-2 [23]. It acts as a substitute for VEGFA, activating the angiogenesis process. Moreover, tFNA, due to its modifiability nature, can be modified with specific single strands to acquire distinct functions. For instance, tFNA modified with miR-2861 can enhance the osteogenic differentiation of MSCs, thus promoting bone repair and regeneration in bone defect models [24]. Consequently, constructing Apt02-tFNA, which combines the functionalities of rapid vascularization and enhanced bone regeneration, presents a promising approach in the field of bone tissue engineering. Additionally, considering the mechanical shortcomings of DNA hydrogels, we introduced FDA-approved polycaprolactone (PCL) [25] as a mechanical support.

Based on the aforementioned, we developed a novel, nucleic acid-based hydrogel, composed of polymer-modified DNA hydrogel and Apt02-tFNA, which can significantly reduce synthesis costs while maintaining biocompatibility and suitability for cell encapsulation. The introduction of Apt02 and tFNA significantly promoted angiogenesis in HUVECs and osteogenic mineralization in BMSCs, respectively. Transcriptome sequencing of these two cell types revealed the specific targeting of Apt02, significantly inhibiting the cytokine-cytokine receptor interaction pathway [26] to mediate endothelial cell proliferation. tFNA targeted and inhibited the Hippo signaling pathway [27,28] to promote osteogenic mineralization in BMSCs. By 3D printing a porous PCL scaffold, we uniformly incorporated the hydrogel into its pores. *In vivo* results demonstrated that the DNA hydrogel containing Apt02-tFNA significantly accelerated bone regeneration, while DNA hydrogel alone also promoted bone formation. This study presents a new type of nucleic acid-based DNA hydrogel, providing a biocompatible material for rapid bone regeneration. It holds promise for clinical treatment of bone defects and further construction of bone organoids.

2. Materials and methods

2.1. Synthesis of DNA acrylamide polymer

The DNA acrylamide polymer is synthesized by reacting acrylamidated DNA with acrylamide (Sigma, #011012963) and sodium acrylate (Sigma, #01346345) under anoxic conditions for a minimum of 12 h, initiating a polymerization reaction. The synthesis system for 150 μl of DNA acrylamide polymer comprises 60 nmol of acrylamidated DNA, 73.125 μl of TE buffer, 30 μl of TBE (5X) buffer (Adamas life, #041111008), 18.9375 μl of a 40w/v% mixture of acrylamide/sodium acrylate (mixed at a 99:1 ratio), 0.3 μl of 10 % Tetramethylethylenediamine (TEMED) (Sigma, #01476459), and 0.3 μl of 10 % Ammonium Persulfate (APS) (Sigma, #01355274). The viscous polymer solution of DNA acrylamide is diluted with seven times its volume of TE buffer, then purified through methanol precipitation. The supernatant is discarded, and the precipitate is resuspended in TE buffer for storage at −20 °C.

2.2. Formation of DNA hydrogel with heat-activated crosslinkers

To prepare the DNA hydrogel, the DNA acrylamide polymer solution is dispersed in 1x TE buffer with 150 mM NaCl solution to a final concentration of 1 wt%, creating two equal precursor solutions. One strand of the DNA crosslinker, equimolar to the acrylamidated DNA, is added to the first tube, while the complementary strand of the DNA crosslinker is added to the second tube. Excess complementary heat-activated blocking strands are then added to each tube and mixed. The precursor solutions are incubated at 4 °C for 1 h, and then the two solutions are mixed and heated to 37 °C to induce gelation.

2.3. Characterization of the DNA hydrogel

The DNA hydrogel was subjected to freeze-drying and gold sputtering, facilitating the examination of its internal morphology via Scanning Electron Microscopy (SEM, JSM-7500F, JEOL, Japan). The hydrogel was molded into cylindrical samples, each approximately 10 mm in diameter and 6 mm in thickness. The mechanical properties of the DNA hydrogel were analyzed using a rheometer (HR20, TA Instruments). Strain sweep tests were conducted to evaluate the storage modulus (G') and loss modulus (G'') across a shear strain range of 0.01–100 %. Furthermore, oscillation frequency sweep tests were performed to determine the corresponding G' and G'' within the frequency range of 0.01–100 $rads^{-1}$. The wettability of the hydrogel was assessed using a contact angle meter (JC2000D1, ZhongChen, Shanghai), with a custom analysis system employed to measure the water contact angle.

2.4. Degradation experiment

The DNA hydrogel containing Apt02-tFNA was freeze-dried to ascertain its dry weight. It was then immersed in α-MEM containing 10

% fetal bovine serum. The samples were retrieved at predetermined intervals, freeze-dried, and reweighed to track changes in dry weight over time.

2.5. Assembly of tFNA

Equimolar concentrations of four predesigned single-stranded DNA (ssDNA) sequences, as outlined in Table S2, were combined in TM buffer. This mixture underwent a denaturation process at 95 °C for 10 min, followed by a rapid cooling phase to 4 °C for 20 min, facilitated by equipment from Sangon, Shanghai, China. The concentration of ssDNA in the solution was precisely quantified using UV spectroscopy. As an exemplar procedure, 96 μl of TM buffer was added to four aliquots of 1 μl ssDNA.

2.6. Synthesis and characterization of Apt02-Modified tFNA

A mixture of three ssDNA strands and one Aptamer02-modified strand was prepared in TM buffer at equimolar concentrations to a final volume of 100 μl, as detailed in Table S2. This mixture was then denatured at 95 °C for 10 min and subsequently cooled to 4 °C for 20 min. The successful synthesis of tFNA was confirmed using polyacrylamide gel electrophoresis (PAGE) and transmission electron microscopy (TEM), ensuring the integrity and accuracy of the aptamer-modified tFNA structures.

2.7. Construction of Apt02-tFNA loaded in DNA hydrogel

The preparation process for the DNA hydrogel loaded with tFNA and Apt02-tFNA follows a similar protocol to that of the standard DNA hydrogel. In this procedure, both tFNA and Apt02-tFNA are physically mixed into the DNA hydrogel precursor solution prior to gelation.

2.8. Fabrication and characterization of the PCL scaffold

The scaffold structure was designed as a “circular" form, a common choice in tissue engineering. The design, upon completion, was imported into a software to create a 6-layer disc-shaped scaffold model. For 3D printing, parameters were set as follows: temperature at 120 °C, dimensions at 15 mm × 15 mm × 1.2 mm, nozzle movement speed at 11 mm/s, and a 0.3 s pause between printing layers. PCL particles were preheated in a high temperature chamber at 120 °C for 20 min to ensure full melting. Following the high-temperature extrusion 3D printing process, uniformly sized circular scaffolds were obtained using a 5 mm punch. The mechanical properties of the DNA hydrogel were then analyzed using a rheometer (HR20, TA Instruments), conducting both strain sweep tests (across a shear strain range of 0.1–100 % to assess storage modulus G′ and loss modulus G″) and oscillatory frequency sweep tests (within a frequency range of 0.1–100 rads-1 to determine corresponding G′ and G″ values).

2.9. The transcriptome sequencing of BMSCs and HUVECs

BMSCs and HUVECs were divided into five groups for culturing. When the cell density reached approximately 70%–80 %, five different groups of extracts were sequentially added to the respective groups. The cells were then cultured for an additional three days. Subsequently, from each group, one million cells were collected for transcriptome sequencing.

2.10. Cultivation of BMSCs and HUVECs

BMSCs were acquired from the China Science Academy’s Type Culture Collection Center (SCSP-402, Shanghai, China). The BMSCs were cultured in Dulbecco’s Modified Eagle Medium (MEM-alpha, C11995500BT, Gibco, USA) supplemented with 10 % fetal bovine serum (Gibco, C2027050, USA) and 1 % penicillin-streptomycin (Gibco, 15140-122, USA). The cells were maintained at 37 °C in a 5 % CO_2 environment. For passaging and seeding, BMSCs were enzymatically dissociated using trypsin and collected by centrifugation.

HUVECs were cultured in endothelial cell-specific growth medium (Lonza, CC-3162, USA). The conditions for HUVECs culture were maintained similarly to those for BMSCs, including the use of 10 % fetal bovine serum and 1 % penicillin-streptomycin in the culture medium.

2.11. Cell viability and metabolic activity assays

The Cell Counting Kit-8 (CCK-8, Beyotime, C0039, China) was employed to assess cell viability and to evaluate the impact of different concentrations of Apt02-tFNA in DNA hydrogels on cell proliferation. DNA hydrogels loaded with Apt02-tFNA were prepared, and equal volumes of serum-free medium were added and incubated for 48 h to obtain the extract. This extract was then mixed with varying volumes of medium to achieve different concentrations. BMSCs and HUVECs were seeded into 96-well plates, followed by the addition of extracts at different concentrations and incubated for 48 h. Subsequently, CCK-8 reagent was added to each well and incubated for 2 h.

Additionally, live-dead staining was utilized to characterize the cell viability in the DNA hydrogel extracts on BMSCs and HUVECs. First, working solutions of Calcein-AM and Propidium Iodide (PI) stains were prepared. The staining solutions of Calcein-AM and PI were diluted in Phosphate-Buffered Saline (PBS) at ratios of 1:500 and 1.5:500, respectively, and then mixed to create the working solution. This working solution was added to the wells containing the samples at a 1:2 vol ratio to the culture medium and incubated at 37 °C for 15 min. Actin-Tracker Green-488 was used to capture cell morphology.

2.12. Effect of hydrogels loaded with Apt02-tFNA on osteogenic differentiation of BMSCs

BMSCs at a density of 1×10^5 cells were seeded into 24-well plates. Following cell adhesion, the medium containing hydrogel extracts was added to culture the BMSCs. Osteogenic-related gene expressions of COL1, BMP2, Osterix, VEGF-1 [29], and OCN were detected using quantitative RT-PCR, with GAPDH serving as the control gene. The specific primer sequences used are listed in Table S1 mRNA was extracted from the respective samples on day 3. Each test was conducted on three distinct samples (n = 3). The $\Delta\Delta Ct$ relative method was used to calculate fold increases in expression. Results were normalized to gene expression levels obtained from BMSCs cultured with PCL scaffold controls.

After culturing BMSCs for 14 days in medium containing hydrogel extracts, Alizarin Red staining was used to characterize the formation of mineralized matrix. BMSCs were first fixed with 4 % paraformaldehyde, followed by staining with Alizarin Red solution to mark the mineralized matrix. Subsequently, a solution of dodecylpyridinium chloride (100 mM) was added to each well to quantify the mineralized matrix. Absorbance at 562 nm was measured using a microplate reader (Thermo 3001, Thermo Scientific, USA).

2.13. Evaluation of the angiogenic activity of DNA hydrogel loaded with Apt02-tFNA in vitro

HUVECs at a density of 1×10^5 were seeded into 24-well plates. After culturing the HUVECs for 3 days in medium containing hydrogel extracts, quantitative RT-PCR analysis was performed to estimate the gene expression of several angiogenic markers, including vWF, SMAD1, ANG-1, FGF and VEGFA, using GAPDH as a control gene. The specific primer sequences used are listed in Table S1, and mRNA was extracted from each sample on the 3rd day. Each test was conducted on three distinct samples (n = 3). The ΔΔCt relative method was used for calculating fold increases in expression. Results were normalized to the gene expression

levels obtained from HUVECs cultured with PCL scaffold controls.

Subsequently, after 3 days of cultivation in medium with extracts from different groups, HUVECs were digested, and 1×10^4 HUVECs were seeded onto a micro-angiogenesis plate containing Matrigel (Corning, USA). After 8 h of culture in endothelial cell growth medium, tube formation by HUVECs was observed under an optical microscope. The formation of HUVECs tubules in the micro-angiogenesis plate was visualized under the bright field of the optical microscope. Photographs of HUVECs in the micro-angiogenesis plate were taken using a microscope, and the number of tubes formed by HUVECs was counted using ImageJ software, with four different views per sample.

2.14. In vivo experiments

The animal procedures adhered to the Guidelines for Care and Use of Laboratory Animals of Shanghai University and received approval from the University's Animal Ethics Committee (YS 2023-160). *In vivo* experiments involved the use of Sprague Dawley rats (male, 8 weeks old) to establish a cranial defect model with a diameter of 5 mm. The rats were euthanized at 4 and 8 weeks post-model establishment, and their skulls were harvested for Microcomputed tomography (μCT) system analysis. Relevant bone parameters such as new bone volume (BV), new bone volume relative to defect volume (BV/TV), and new bone density (BMD) were calculated. For the observation of cellular and tissue responses to various treatments, skull tissue was embedded in paraffin for sectioning. Staining procedures, including Hematoxylin and Eosin (H&E) staining and Masson's trichrome staining, were performed. Immunohistochemical analyses for CD31, OPN, and OCN, as well as immunofluorescence for CD31 and OCN, were also conducted.

2.15. Statistical analysis

Data are presented as means ± standard deviation (SD). Statistical evaluations were performed using one-way Analysis of Variance (ANOVA) followed by post hoc tests for multiple comparisons. A p-value of less than 0.05 was considered to indicate statistical significance. Levels of significance are denoted as: $*p < 0.05$, $**p < 0.01$, and $***p < 0.001$.

3. Results and discussion

3.1. Preparation and characterization of DNA hydrogel

In this study, we initiated the preparation by dispersing anchor DNA strands in an acrylamide solution, followed by a polymerization reaction to create an acrylamide polymer with multiple DNA strands as the main chain. Utilizing the principle of Watson Crick base pairing, DNA crosslinkers capable of complementary interaction with the anchor DNA were employed to connect the acrylamide polymers, resulting in the synthesis of a DNA hydrogel. A total of 64 crosslinkers were used for base pairing with the anchor DNA, enhancing the uniformity of the resulting DNA hydrogel. The process incorporated heat-activated blocking strands, which at 4 °C bind with crosslinkers based on complementary base pairing, thereby inhibiting DNA hydrogel formation. However, at 37 °C, these strands dissociate from the crosslinkers, facilitating the formation of the DNA hydrogel (Fig. S1a). This temperature-responsive self-assembly characteristic renders it particularly suitable for human application (Fig. 1a). It is important to note that traditionally used thermoresponsive materials include Poly(N-isopropylacrylamide) (PNIPAM), Polyethylene Glycol (PEG), and Polydimethylsiloxane (PDMS), which are capable of altering their physical or chemical properties at specific temperatures. For instance, polymer materials incorporating Y-type DNA into PNIPAM can undergo a phase transition near the human body temperature [30]. However, in our experiments, the formation of DNA hydrogels in response to temperature changes is mediated by the binding and dissociation of DNA strands. Moreover, the components of the DNA hydrogels used in our study are not traditional thermoresponsive materials. Compared to conventional thermoresponsive materials, our DNA hydrogels exhibit superior biocompatibility and safety.

Rheological testing of the DNA hydrogel (Fig. 1d and e) revealed that within a strain range of 0.01%–100 % and a frequency sweep from 0.01 to 100 rad/s, the hydrogel's elastic shear storage modulus (G′) consistently exceeded its viscous shear loss modulus (G″), indicating the DNA hydrogel exhibits relatively stable structure. The study methodically investigated the viscosity of the hydrogel as a function of shear rate, spanning a range from 0.01 to 100 s^{-1}. This analysis revealed a pronounced shear-thinning behavior, characterized by a decrease in viscosity upon the application of shear stress. Such a response is indicative of the adaptive rheological properties of hydrogel, particularly demonstrating superior injectability. This characteristic is pivotal in biomechanical applications, where ease of application and adaptability to physiological shear conditions are essential. The shear-thinning profile of hydrogel underscores its potential for effective delivery and integration within biological systems, offering substantial benefits in biomedical applications requiring precise and minimally invasive administration (Fig. 1f). Further characterization using Scanning Electron Microscopy (SEM) of the freeze-dried hydrogel revealed a porous microstructure within the DNA hydrogel (Fig. 1b), which could facilitate the encapsulation of tFNA. The DNA hydrogel's injectability was evidenced by its ability to rapidly recover its initial state within seconds during shear-thinning and reforming processes, even forming various letters (Fig. 1a), indicating remarkable self-healing properties.

The biodegradability of the DNA hydrogel is crucial for its therapeutic [31] applications. To this end, rabbit actin at a final concentration of 300 μg/mL was incorporated during the physical mixing of the DNA hydrogel, which sustained 90 % of the DNA hydrogel content after three weeks of incubation in 10 % fetal bovine serum medium (Fig. 1c). Compared to traditional DNA hydrogels, the synthesized DNA hydrogel in this study exhibited significantly extended degradation, making it suitable for a variety of biological processes and particularly as a carrier material for bone repair studies requiring prolonged durations. Additionally, the crosslinkers in the DNA hydrogel, which play a pivotal role in connection, can be designed with varying quantities and lengths of complementary strands, yielding different hydrogel strengths. This editability of the DNA hydrogel meets diverse experimental objectives. The structural stability of DNA hydrogels, combined with their excellent injectability and prolonged degradation time, renders them particularly suitable for encapsulating small molecule active substances in bone repair applications. Such characteristics are crucial in the early stages of bone regeneration, where the extended, gradual release of therapeutic agents plays a significant role. The longevity of the hydrogel's degradation process ensures a sustained release of these molecules, maintaining a consistent therapeutic presence at the site of bone repair. This controlled release mechanism not only maximizes the efficacy of the active substances but also minimizes potential systemic side effects, making DNA hydrogels a promising vehicle for targeted bone regeneration therapies.

3.2. Fabrication and characterization of the DNA hydrogel-scaffold

The foundation of successful bone regeneration lies in the effective promotion of osteogenesis. tFNA, assembled from four specifically designed oligonucleotide strands (S1, S2, S3, S4) [32], enhances the differentiation potential of stem cells towards osteoblasts (Fig. 1g). Additionally, robust angiogenic capability, vital for supplying oxygen and nutrients for bone growth, is facilitated by Apt02-tFNA, composed of four oligonucleotides (S1, S2, S3, Apt02-S4) self-assembled to promote endothelial cell proliferation and angiogenesis. Apt02-tFNA was synthesized and confirmed via polyacrylamide gel electrophoresis (PAGE) (Fig. 1h), where the mobility of the five oligonucleotides in Apt02-tFNA was observed to be faster compared to tFNA and

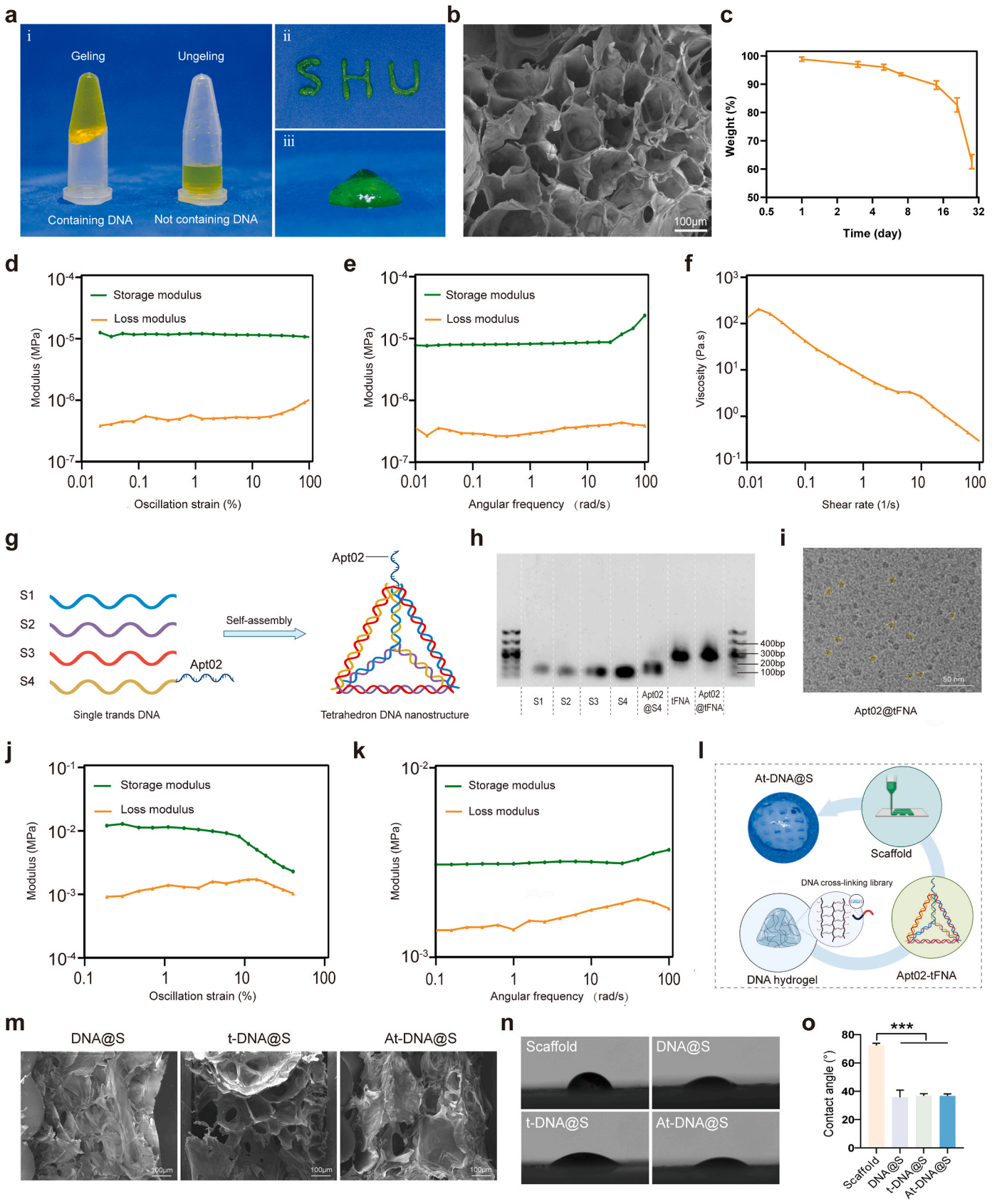

Fig. 1. Characterization of all-nucleic acid-based DNA hydrogel. (a) Photograph of hydrogel/DNA hydrogel. (b) SEM representative images of DNA hydrogel. (c) The degradation of DNA hydrogel. (d) Modulus vs. Stress of DNA Hydrogel. (e) Modulus vs. Frequency of DNA Hydrogel. (f) Viscoelasticity vs. Shear Rate of DNA Hydrogel. (g) Schematic diagram of DNA framework nucleic acid synthesis. (h) Agarose gel electrophoresis for Apt02@tFNA identification. (i) TEM representative images of Apt02@tFNA. (j) Modulus vs. Stress of PCL scaffold. (k) Modulus vs. Frequency of PCL scaffold. (l) Schematic diagram of Apt02@tFNA synthesis. (m) SEM representative image of different DNA hydrogel composite scaffold. (n) Water droplets and (o) contact angles on the material.

aptamer-tFNA, with aptamer-tFNA exhibiting the slowest mobility. Transmission Electron Microscopy (TEM) was utilized to determine the size of Apt02-tFNA, which was found to be less than 10 nm (Fig. 1i). These results indicate successful assembly of Apt02-tFNA and tFNA. Incorporating Apt02 in the DNA hydrogel allows for sustained release of therapeutic agents, making it applicable for bone repair treatments.

PCL is known for its excellent bioprintability and biocompatibility, making it suitable for fabricating biologically safe scaffolds for *in vivo* use. Rheological testing robustly validated the stable physical properties of the material. This testing confirmed its ability to maintain structural integrity and rapidly return to its original configuration, even under cyclic or varying load conditions. Such resilience is crucial for enduring the dynamic mechanical environments typically encountered in bone repairing, demonstrating the material's reliability and adaptability (Fig. 1j and k). In this study, a cylindrical scaffold with a diameter of 5 mm and a thickness of 1.2 mm was designed and printed, then physically mixed with tFNA/Apt02-tFNA in the DNA hydrogel precursor solution to form a composite DNA hydrogel-scaffold containing tFNA/Apt02-tFNA (Fig. 1l). Moreover, after combining the PCL scaffold with the DNA hydrogel, there was no significant change in its mechanical properties (Figs. S1b–c). This implies that the scaffold maintains its robust supportive function, providing a stable structure and favorable adhesion points for materials and cells during the bone formation process. SEM revealed that the DNA hydrogel effectively intermingled with the scaffold, maintaining appropriate porosity without significant changes in pore size due to the addition of tFNA/Apt02-tFNA (Fig. 1m). The presence of tFNA/Apt02-tFNA within the scaffold enhances osteogenesis and angiogenesis, facilitating new bone formation. Subsequently, the hydrophilicity of each material group was assessed. The PCL displayed a relatively hydrophobic nature with an average contact angle of about 72.3°. However, the DNA hydrogel, DNA hydrogel loaded with tFNA, and DNA hydrogel loaded with apt-tFNA exhibited significantly reduced average contact angles of 35.8°, 36.9°, and 36.8°, respectively (Fig. 1n and o), demonstrating enhanced hydrophilicity capable of effectively wetting the PCL scaffold. The all-nucleic acid-based hydrogel, when integrated with the composite scaffold, exhibits a tight adherence to the scaffold structure without any alteration in its physical properties. This observation indicates that the hydrogel maintains structural stability, which is anticipated to play a significant role in subsequent bone repair processes. The unaltered physical characteristics of the hydrogel after its composite formation suggest that it can reliably function in the physiological environment of bone repair. This stability is crucial for ensuring the hydrogel's effectiveness in facilitating osteointegration and promoting tissue regeneration [33,34]. The ability of the hydrogel to maintain its integrity while in close contact with the scaffold underlines its potential as a viable medium for supporting bone healing and regeneration.

3.3. DNA hydrogel-scaffold enhances in vitro angiogenesis

The study was structured into five groups: Control, Scaffold, DNA hydrogel + scaffold (DNA@S), DNA hydrogel + tFNA + scaffold (t-DNA@S), and DNA hydrogel + Apt-tFNA + scaffold (At-DNA@S). The DNA hydrogel-scaffold components of each group's extract are different. The extracts from different groups contain parts or all of the components of DNA hydrogel, tFNA, and Apt02-tFNA. Firstly, in order to identify the optimal concentrations of Apt02-tFNA for enhancing the proliferation of HUVECs, we used a CCK8 assay kit to evaluate the effects of DNA hydrogel extracts containing different concentrations of Apt02-tFNA on HUVECs proliferation. Results (Fig. S2c) indicated that HUVECs proliferation was most robust at a concentration of 32 nmol L^{-1} of Apt02-tFNA in the extracts. Subsequently, the effect on the biosafety of HUVECs at this concentration was examined. Live-dead staining showed that HUVECs in each group were alive and the components in the extract did not induce harm (Fig. S2a). Similarly, cytoskeletal staining revealed normal morphology in all groups, indicating that the components did not adversely affect cellular viability (Fig. 2a and b). This suggests that the DNA hydrogel extracts at this concentration were non-toxic to the cells.

Further, Apt02 has VEGF-like functions in promoting angiogenesis, and we subsequently evaluated the effects of each group on the capability of blood vessel formation. Wound healing assays were employed to assess HUVECs migration behavior (Fig. 2c and d). Initially, consistent and regular scratches approximately 500 μm wide were made in HUVECs, and after 24 h of incubation with different group extracts, the Control group showed a 35 % increase in scratch area, while the Scaffold group showed a 37 % increase, not significantly different from the control. However, the At-DNA@S group showed the most significant increase in closed area, reaching 92 %. These results indicate that Apt02-tFNA can promote vascular migration effectively.

Furthermore, we evaluated the expression of angiogenesis-related genes in each experimental group (Fig. 2g). Compared to the Control, the At-DNA@S group showed increased expression of SMAD 1, VEGFA, VWF, ANG1, and FGF genes, possibly due to the high expression of Apt02 promoting VEGF release. Additionally, the impact of different groups on HUVECs tube formation was assessed (Fig. 2e and f). These experimental results demonstrate that the At-DNA@S composite material can significantly promote angiogenesis. The aforementioned results corroborate our anticipated findings, indicating that Apt02-tFNA can effectively promote angiogenesis. This capability is crucial for providing nutritional support during the rapid vascularization phase of bone regeneration. The enhancement of angiogenesis by Apt02-tFNA aligns with the fundamental understanding that efficient blood supply is vital for the successful regeneration of bone tissue. By facilitating the formation of a vascular network, Apt02-tFNA not only supports the transport of essential nutrients and oxygen to the regenerating site but also aids in the removal of waste products, thereby creating an optimal environment for bone healing and growth. This finding underscores the potential of Apt02-tFNA as a key component in bone tissue engineering strategies, particularly in scenarios where accelerated vascularization is critical for the healing process.

3.4. Transcriptome sequencing of HUVECs

To confirm and expand upon the aforementioned results, we conducted a whole transcriptome RNA sequencing. Utilizing UpSet analysis [35], we identified gene sets of interest between various groups. As illustrated (Fig. 3a), the largest gene set was induced by At-DNA@S versus Scaffold (n = 3671), followed by At-DNA@S versus t-DNA@S (n = 1702) and t-DNA@S versus Scaffold (n = 656). The larger gene set for the At-DNA@S and Scaffold combination compared to others indicates that the incorporation of Apt02-tFNA significantly influenced angiogenic gene expression. The substantial difference between At-DNA@S and t-DNA@S underscores the distinct impact of Apt02, relative to tFNA alone, on angiogenesis. Subsequently, we conducted KEGG analysis to explore the molecular biological mechanisms of different expression genes (DEGs) affecting HUVECs angiogenic differentiation. In the t-DNA@S VS DNA@S combination (Fig. 3b and c), upregulated genes were found to function through multiple pathways, predominantly affecting Carbohydrate metabolism within Global and overview maps. Further investigation identified five key pathways: Metabolic pathways, Proteasome, Oxidative phosphorylation, DNA replication, and Cell cycle. The Metabolic pathways were particularly crucial; based on our findings, upregulated genes influenced cell cycle and cellular metabolism, thus promoting HUVEC tubulogenesis. Downregulated genes functioned by attenuating pathways like the Hippo signaling pathway (Fig. 3d and e), Steroid biosynthesis, Endocytosis, Insulin signaling pathway, and Terpenoid backbone biosynthesis.

Analysis of the At-DNA@S and t-DNA@S combination revealed that (Fig. 3f andg), post-Apt02 introduction, upregulated genes were distributed in Metabolism within Global and overview maps, impacting

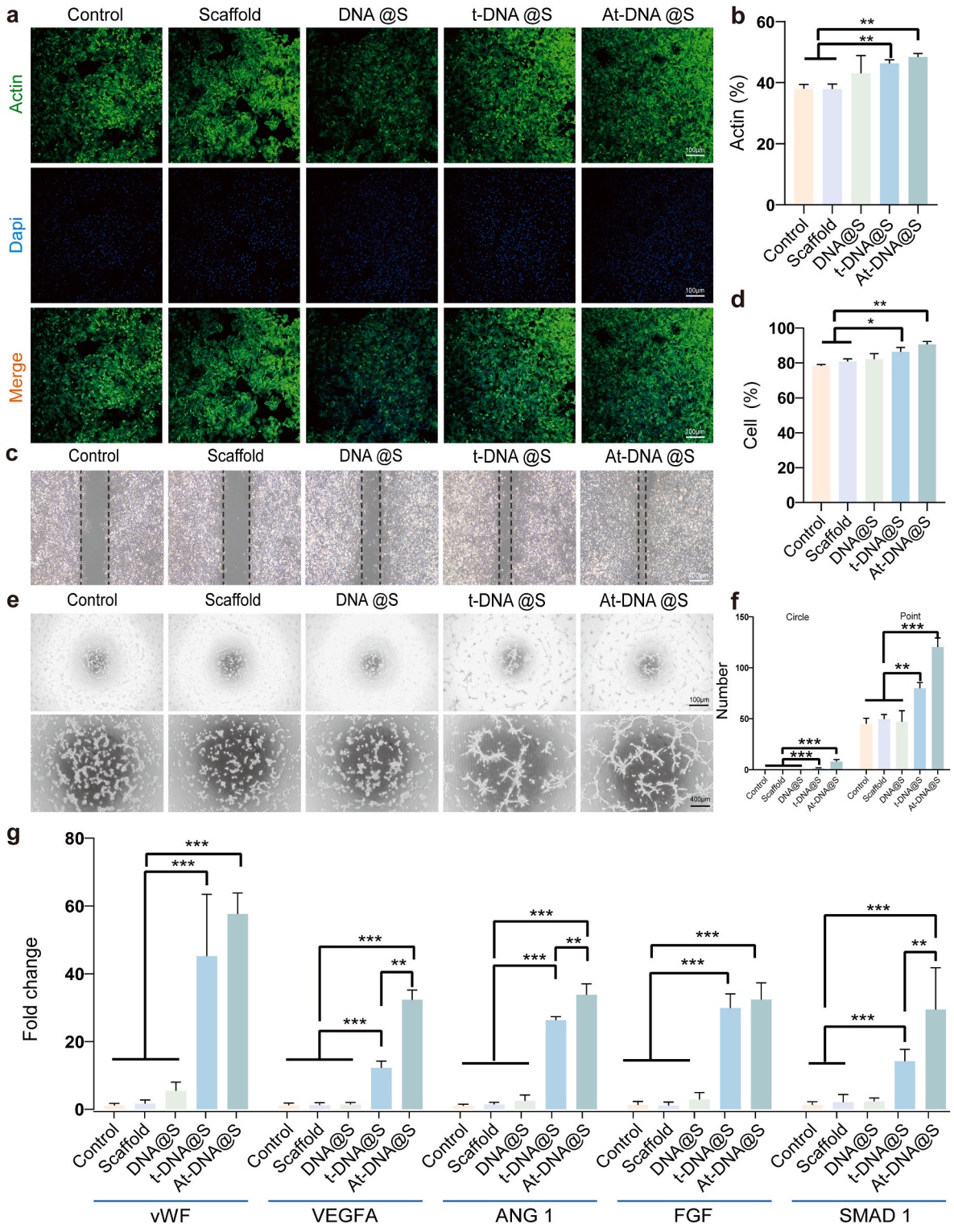

Fig. 2. DNA hydrogel-scaffold enhances *in vitro* angiogenesis. (a) The cytoskeleton of HUVECs after treated for 48 h. (b) Quantitative analysis of the cellular cytoskeleton. (c) Cell scratch experiment to verify the migration ability of HUVECs after treated for 24 h. (d) Quantitative analysis of migration. (e) Optical images of the capillary-like network formed by HUVECs after treated for 8 h on Matrix gel with the specimen-conditioned medium. (f) Quantification of points and circles formed by HUVECs after treated 8 h on the gel. (g) qRT-PCR experiments were conducted to validate the relative expression levels of genes (VWF, VEGFA, ANG 1, FGF, and SMAD 1) in each experimental group. *$p < 0.05$, **$p < 0.01$, and ***$p < 0.001$.

DNA replication, Proteasome, Cell cycle, Oxidative phosphorylation, and Glutathione metabolism pathways. Major downregulated pathways included the Hippo signaling pathway, Adipocytokine signaling pathway, PPAR signaling pathway, Apoptosis, and Rap1 signaling pathway (Fig. 3h and i). The Hippo signaling pathway, known for its role in cellular proliferation, can lead to excessive cell proliferation if unactivated in tissues, as YAP binds to transcription factors [36]. Its attenuation may promote enhanced cellular growth. The Rap1 signaling pathway, involved in vital cellular processes like cell adhesion, communication, migration, polarization, proliferation, and survival,

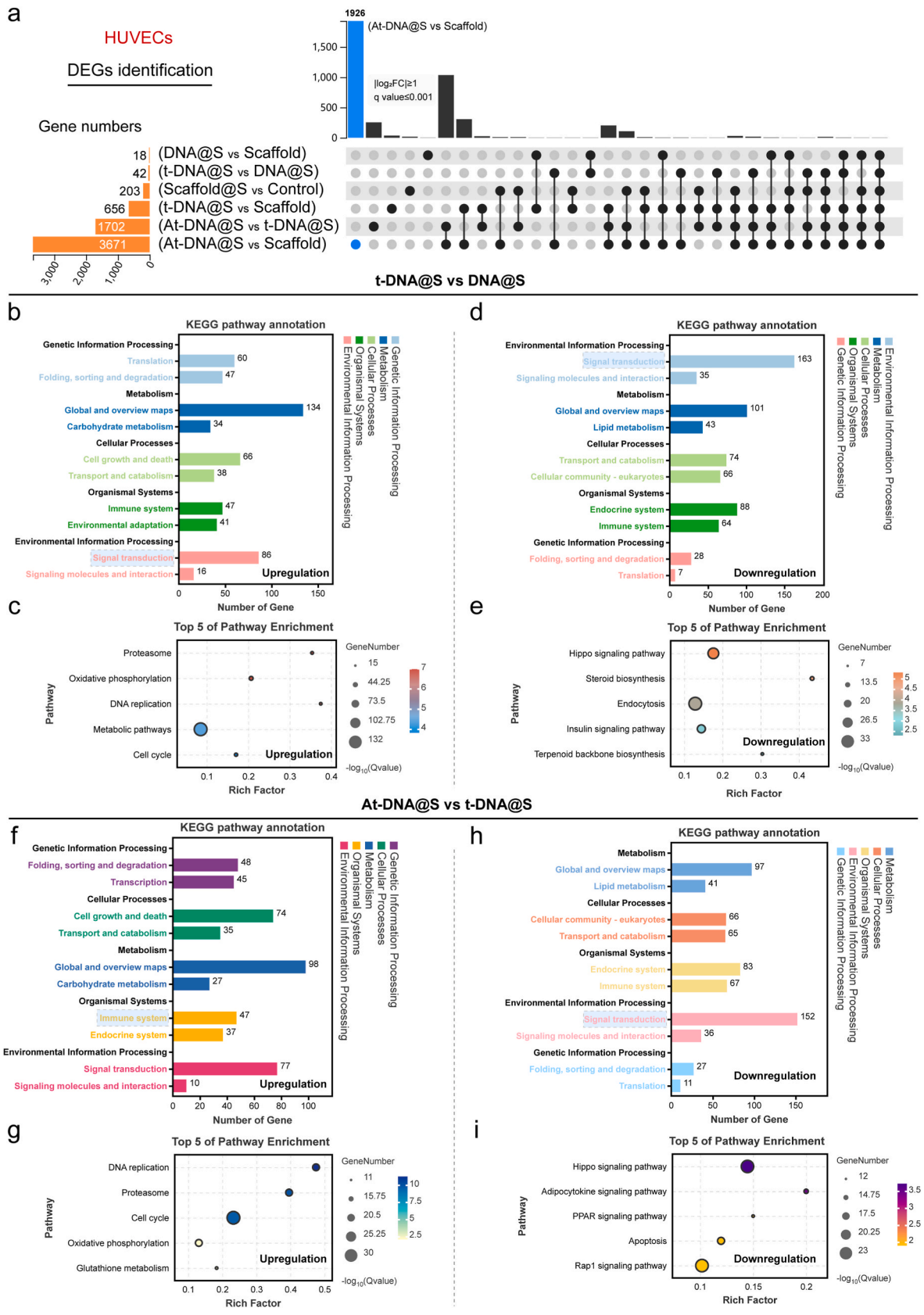

Fig. 3. Transcriptome sequencing analysis of HUVECs. (a) DEGs were identified to determine the differential gene sets by all possible combinations of patterns. (b and c) Upregulated pathway analysis and TOP 5 pathway enrichment of t-DNA@S VS DNA@S. (d and e) Down-regulated pathway analysis and TOP 5 pathway enrichment of t-DNA@S VS DNA@S. (f and g) Upregulated pathway analysis and TOP 5 pathway enrichment of At-DNA@S vs t-DNA@S. (h and i) Down-regulated pathway analysis and TOP 5 pathway enrichment of At-DNA@S vs t-DNA@S.

regulates the secretion of interleukin-1β (IL-1β) and tumor necrosis factor-α (TNF-α). Consequently, Apt02 can promote cellular metabolic and replication processes, and to some extent, mitigate cell migration and inflammatory responses, ultimately enhancing HUVEC proliferation, differentiation, and angiogenesis.

3.5. DNA hydrogel-scaffold enhances in vitro osteogenesis

To determine the optimal concentration for culturing, various concentrations of DNA hydrogel extracts were mixed with the medium and co-cultured with BMSCs. Through the CCK-8 assay (Fig. S2b), we observed that BMSCs proliferation was most effective at a concentration of 32 nmol L−1 of tFNA and Apt02-tFNA in the extracts. Subsequently, the biocompatibility of each group's extract with BMSCs was assessed at this concentration. Live-dead staining experiments revealed that, compared to the blank control group, all other groups showed good cell viability with no significant differences, indicating the non-toxic nature of the extracts to BMSCs. Further assessment of cell morphology through cytoskeletal staining (Fig. 4a and b) showed that cells in all groups maintained normal morphology, unaffected by the components in the extracts. This implies good biocompatibility of the DNA hydrogel scaffold with BMSCs.

In the process of bone regeneration, mineralization plays a crucial role, where the extracellular matrix deposits calcium phosphate crystals [37]. The extent of mineralization was assessed using Alizarin Red staining, which turns red upon binding to mineralized matrix (Fig. 4c and d). Compared to the Control and Scaffold groups, increased Alizarin Red staining was observed in the DNA@S, t-DNA@S, and At-DNA@S groups. Further analysis revealed a greater number of mineralized nodules in the At-DNA@S group compared to the DNA@S group. Alkaline phosphatase (ALP), a glycoprotein synthesized and secreted by osteoblasts, hydrolyzes phosphoesters during osteogenesis, providing necessary phosphate for hydroxyapatite deposition. The ALP content, an indicator of osteogenic differentiation, was measured (Fig. 4c–e). Increased ALP staining was noted in the At-DNA@S, t-DNA@S, and DNA@S groups compared to the Control and Scaffold groups, with the At-DNA@S group exhibiting more intense staining. These results indicate that DNA hydrogel, tFNA, and Apt02-tFNA can promote osteogenic differentiation. The addition of tFNA and Apt02-tFNA further enhances the bone-forming effect of the DNA hydrogel. Consequently, the At-DNA@S composite scaffold has an accelerated role in promoting osteoblast differentiation and bone formation.

Furthermore, this study quantitatively evaluated the expression of osteogenesis-related genes (BMP2, OSX, COL-1, OCN) (Fig. 4f). Compared to the blank scaffold group, the expression levels of BMP2, OSX, COL-1, OCN genes significantly increased in the DNA@S, indicating that DNA hydrogel, tFNA, and Apt02-tFNA stimulate osteogenic gene expression and promote osteogenic differentiation. Additionally, tFNA and Apt02-tFNA significantly increased osteogenic gene expression and enhanced osteogenesis. To further verify the expression of osteogenic-related genes, we quantitatively analyzed the expression of these genes in BMSCs cultured under different group conditions for 14 days. The results revealed a gene expression trend similar to that observed during the initial three days, with an additional increase in the expression levels of osteogenic-related genes (Fig. S5a). Therefore, the Apt02-tFNA and DNA hydrogel in the DNA hydrogel scaffold have a synergistic effect in accelerating the osteogenic differentiation process of BMSCs.

3.6. Transcriptome sequencing of BMSCs

To validate the aforementioned results, we conducted comprehensive transcriptome RNA sequencing to unveil the potential biomolecular mechanisms behind the material-induced osteogenesis. We identified potential intergroup combinations to determine specific gene sets potentially induced, and assessed the size of these gene sets of interest using UpSet. As anticipated, the largest gene set was induced by At-DNA@S versus Scaffold (n = 9643), followed by t-DNA@S versus Scaffold (n = 9259), DNA versus Scaffold (n = 9122), and At-DNA@ versus t-DNA@S (n = 3) (Fig. 5a). The size of this gene set was substantially larger than other combinations, suggesting the significant impact of Apt02-tFNA incorporation and its varying levels on bone gene expression. Additionally, the introduction of tFNA and DNA also affected osteogenic gene expression to a certain degree. Interestingly, the expression difference between At-DNA and vs t-DNA@S groups was minimal and not statistically significant, corroborating our earlier findings that the addition of Apt02 did not enhance osteogenic capabilities compared to tFNA alone. KEGG pathway analysis of the DNA@S vs Scaffold group revealed that upregulated DEGs primarily functioned through signal transduction in environmental information processing (Fig. 5b and c), with further studies indicating that DEGs could affect osteogenesis through the PI3K-AKT pathway. The PI3K-AKT pathway is a critical and classical signaling pathway, playing a key role in osteoblast differentiation and bone formation [38]. Upon an in-depth analysis of the heatmap data (Fig. S3), notable molecular interactions were observed in the DNA@S group compared to the Scaffold group. Specifically, a marked downregulation of genes such as Mmp14, Mmp3, Mmp9, Ripk3, and Edn1 suggests a significant suppression of the TNF signaling pathway. Additionally, the reduced expression of genes Il17rb, Il17f, Il1b, Il6, and Cxcl6 indicates a targeted inhibition of the IL-17 signaling pathway. A similar trend was observed in the NF-κB signaling pathway, evidenced by the downregulation of Cxcl12, Syk, Traf1, Traf2, Bcl2a1, and Cd40. This pattern elucidates the anti-inflammatory potential of the DNA hydrogel, highlighting its role in attenuating inflammatory pathways such as TNF, IL-17, and NF-κB, thereby fostering an environment conducive to BMSCs survival and osteogenic differentiation, essential for effective bone regeneration.

Thus, in our experiment, the DNA hydrogel could promote osteogenic differentiation and bone formation by upregulating genes that activate the PI3K-AKT pathway. In the analysis of downregulated genes, DEGs primarily affected signal transduction in environmental information processing and functioned through the IL-17 and TNF signaling pathways (Fig. 5d and e). This suggests that the DNA hydrogel's reduction of inflammatory responses may play a role in bone formation. The addition of tFNA effectively enhanced the osteogenic action of the DNA hydrogel. In the t-DNA@S and DNA@S combinations, upregulated genes mainly impacted signal transduction in environmental information processing (Fig. 5f and g). Apart from the PI3K-AKT pathway, the MAPK signaling pathway also played a significant role [39]. Analysis of downregulated genes revealed that attenuation of the Complement and coagulation cascades, Chemokine signaling pathway [40], and Cytokine-cytokine receptor interaction [41] could reduce inflammatory responses and lower immune reactions (Fig. 5h and i). Contrasting these findings (Fig. S4), the tFNA@S group exhibited an upregulation in genes associated with key cellular pathways. Genes like Spp1, Sv2a, Sv2b, Lamc2, and Lamb2 were upregulated, signifying an enhanced ECM-receptor interaction pathway. Furthermore, genes Fgf10, Pdgfra, Angpt1, Tlr2, and Jak3 showed increased expression, indicative of an activated PI3K-Akt signaling pathway. The upregulation of Ap3k3, Tk3, Apk13, Ak1, and Raf2 genes pointed to an elevated MAPK signaling pathway. These observations suggest tFNA's pivotal role in modulating cellular dynamics by augmenting pathways like ECM-receptor interaction, PI3K-Akt, and MAPK, crucial in orchestrating cellular proliferation, differentiation, and ultimately, advancing bone tissue formation. These findings suggest that DNA hydrogel and tFNA may promote bone formation by mitigating inflammation through different pathways.

3.7. DNA hydrogel-scaffold enhances in vivo osteogenesis

The final phase of our study involved *in vivo* animal experiments using the Sprague Dawley (SD) rat cranial defect model to evaluate the regenerative capabilities of the DNA hydrogel-scaffold (Fig. 6a). We

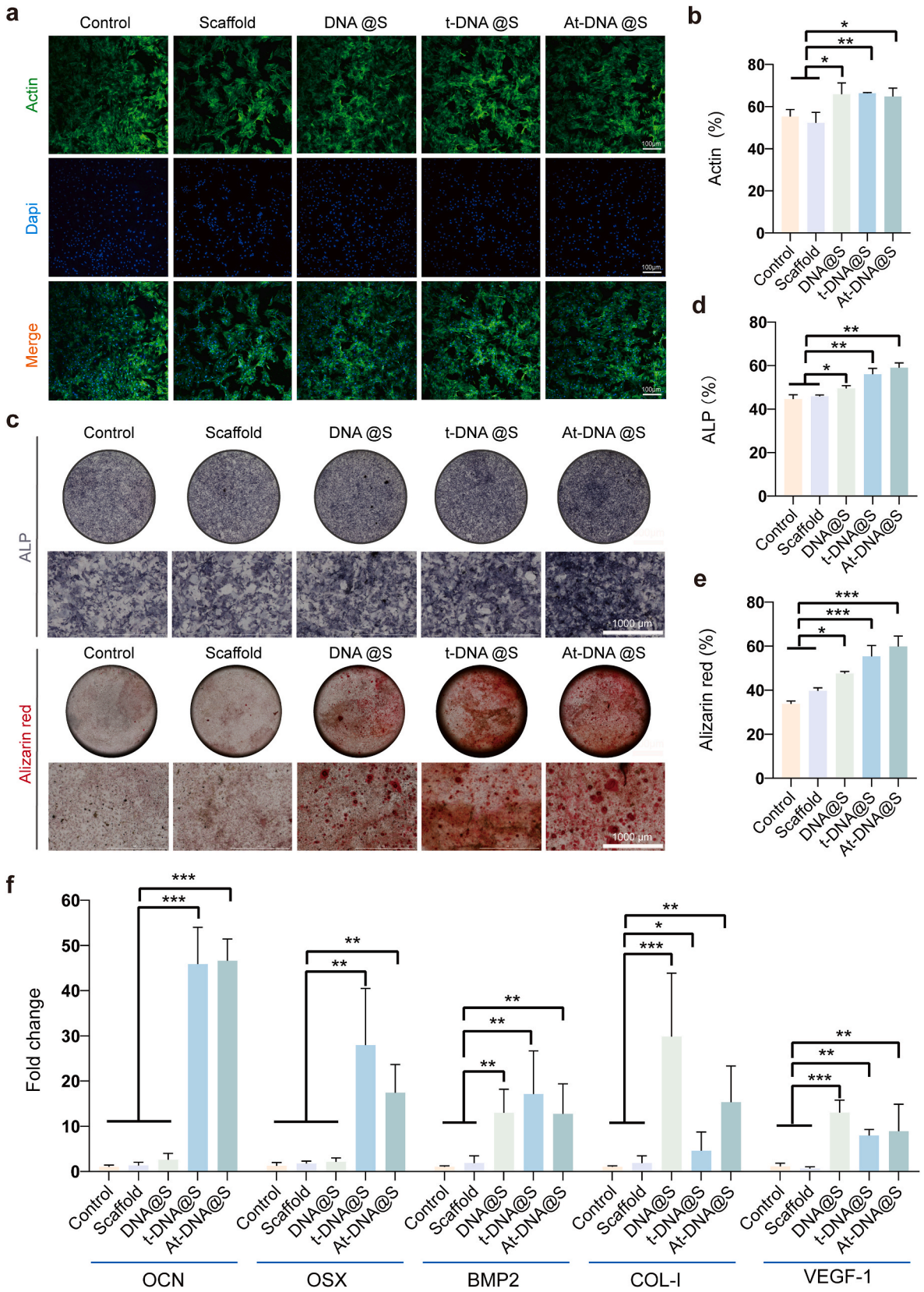

Fig. 4. DNA hydrogel-scaffold enhances *in vitro* osteogenesis. (a) The cytoskeleton of BMSCs after treated for 48 h. (b) Quantitative analysis of the cellular cytoskeleton. (c) ALP staining (up) and Alizarin Red staining (down) after BMSCs were treated with the additive for 14 days. (d and e) Quantitative analysis of ALP and Alizarin Red staining. (f) qRT-PCR experiments were conducted to validate the relative expression levels of genes (OCN, OSX, BMP2, COL-1, and VEGF-1) in each experimental group. *p < 0.05, **p < 0.01, and ***p < 0.001.

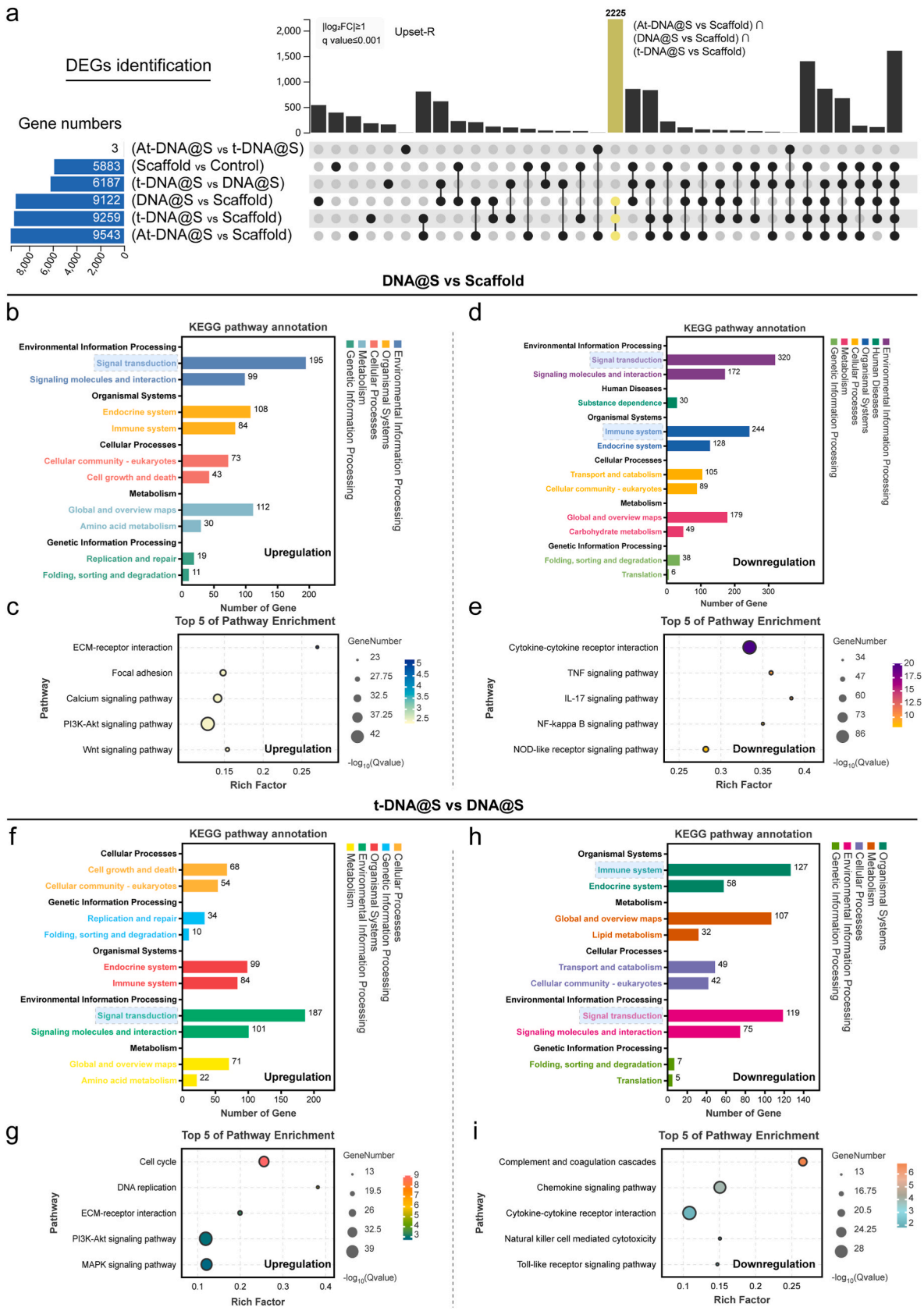

Fig. 5. Transcriptome sequencing analysis of BMSCs. (a) DEGs were identified to determine the specifically induced gene sets by all possible combinations of patterns. (b and c) Upregulated pathway analysis and TOP 5 pathway enrichment of DNA@S vs Scaffold. (d and e) Down-regulated pathway analysis and TOP 5 pathway enrichment of DNA@S vs Scaffold. (f and g) Upregulated pathway analysis and TOP 5 pathway enrichment of t-DNA@S vs DNA@S. (h and i) Down-regulated pathway analysis and TOP 5 pathway enrichment of t-DNA@S vs DNA@S.

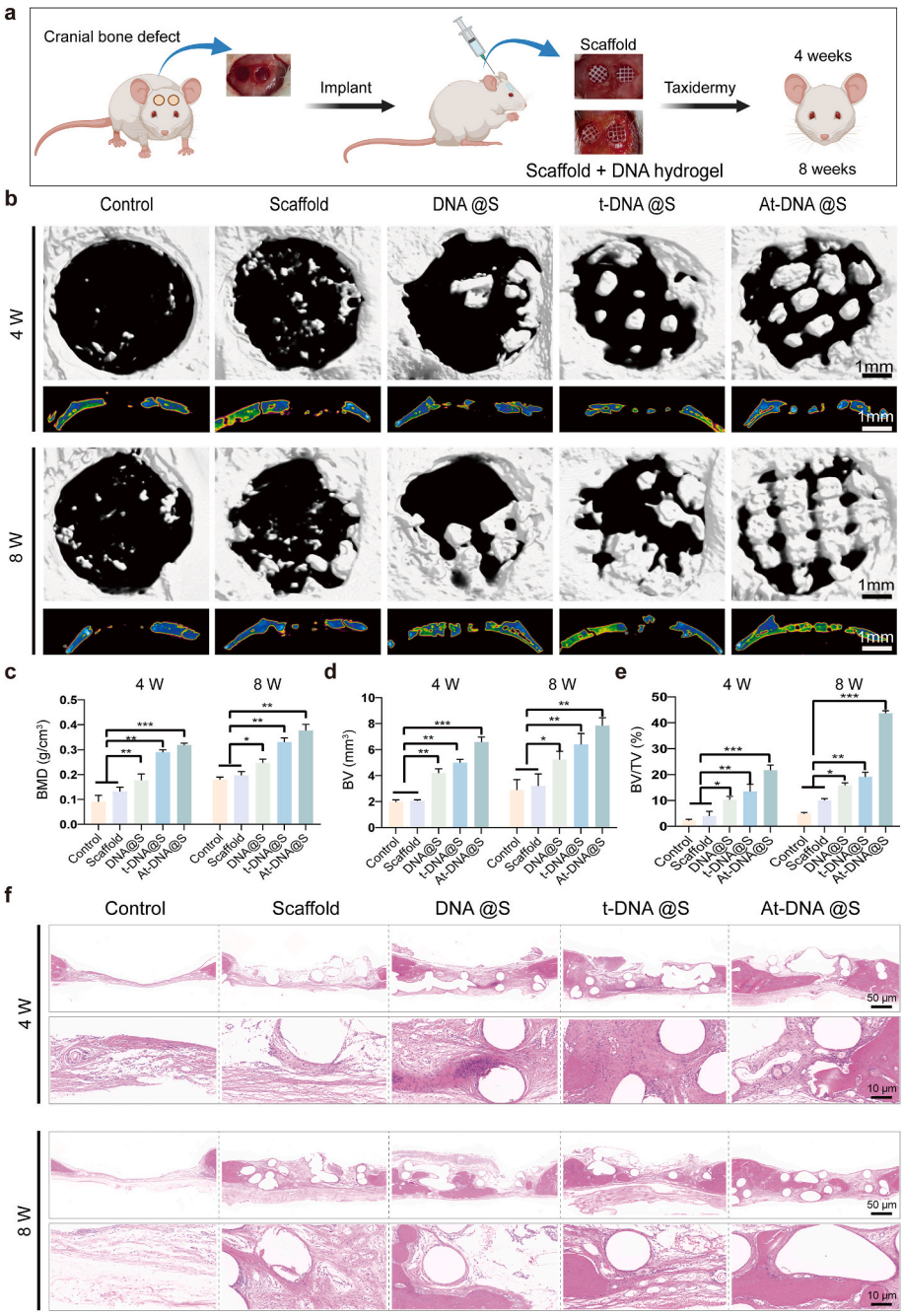

Fig. 6. ***In vivo*** **bone defect repair facilitated by the gel-scaffold constructs.** (a) Schematic illustration of mouse cranial defect and treatment. (b) Micro-CT images depict cranial defects treated with constructs, encompassing both cross-sectional and longitudinal views. (c-e) Quantitative assessment of osteogenesis-related metrics, with BV indicating the volume of new bone, TV indicating the total volume of the defect, and BMD indicating the density of new bone. (f) Histological images stained with H&E exhibit cranial defects following the implantation of scaffold constructs for 4 and 8 weeks. *$p < 0.05$, **$p < 0.01$, and ***$p < 0.001$.

assessed cranial repair at two time points: 4and 8 weeks post-injury. μCT reconstruction was employed to assess bone regeneration at the defect sites (Fig. 6b). New bone growth was observed at the edges of the defect and along the edges of the scaffold within its pores. The Control group showed no significant new bone formation at the defect site, whereas the Scaffold group exhibited increased new bone formation due to appropriate osteoconductivity. Bone formation progressively increased in the DNA@S, t-DNA@S, and At-DNA@S groups, significantly surpassing both the PCL group and the blank control. Consistent with the qualitative assessment, quantitative analysis was conducted for bone volume (BV), the ratio of new bone volume to defect volume (BV/TV), and bone mineral density (BMD) (Fig. 6c–e). At 8 weeks, the new bone volume in the DNA@S was higher than in the Control and Scaffold groups, while the At-DNA@S exhibited the highest new bone volume. Similarly, the BMD of the At-DNA@S and DNA@S groups was significantly greater than in the Control group. Additionally, trabecular number (Tb.N), trabecular thickness (Tb.Th), and trabecular separation (Tb.SP) were also quantitatively analyzed (Figs. S5b–d). Compared to the Scaffold group, both the At-DNA@S and t-DNA@S groups demonstrated a significant increase in the number of trabeculae, along with a reduced spacing between trabeculae. These findings suggest that the DNA hydrogel enhances bone tissue regeneration, and the addition of Apt02-tFNA further augments bone formation.

Hematoxylin and eosin (H&E) staining was used to evaluate new

bone formation (Fig. 6f). The Control group showed substantial fibrous tissue without new bone formation, whereas the Scaffolds provided a porous structure and the DNA hydrogel exerted some osteogenic effect, but bone formation was limited. The addition of tFNA and especially Apt02-tFNA markedly increased new bone formation. Masson's trichrome staining, used for collagen fiber identification, showed blue and red coloration for new and mature bone matrix, respectively (Fig. 7a). The At-DNA@S group exhibited the most effective bone formation, with new bone embedding into the pores of the Scaffold, forming a mixed layer of material and bone that interlocked to create a stable structure. The At-DNA@S group recruited numerous BMSCs for bone formation, further enhancing new bone growth.

In the process of bone formation, osteocalcin (OCN), runt-related transcription factor 2 (RUNX2), a transcription factor indicative of pre-osteoblastic cells, and osteopontin (OPN), a protein present at the onset of mineralization, serve as key markers. Immunohistochemical qualitative characterization of OCN and OPN expression in the bone defect, as well as immunofluorescence assessment of RUNX2 expression, were conducted to study the bone repair capabilities of At-DNA@S. At both time points (Fig. 7b–d), the Control showed no significant difference in OCN positive expression. At 4 and 8 weeks, the DNA@S displayed noticeable brown-yellow areas, i.e., OCN and OPN positive expression zones, especially in the At-DNA@S group (Figure s6b, s6e-f). Similarly, the intensity of red fluorescence, indicating RUNX2 positive expression, was higher in the At-DNA@S group compared to others (Fig. 8b, 8e-f). These results suggest that Apt02-tFNA and DNA hydrogel synergistically promote the formation of bone mineral matrix in the bone defect area. Analysis of CD31 immunofluorescence and immunohistochemistry images showed that the area of CD31 positive expression recruited around the new bone matrix by At-DNA@S was significantly greater than in other groups, indicating the VEGFA-like function of Apt02 in effectively promoting angiogenesis, playing a vital role in bone matrix mineralization and new bone formation (Fig. 8a, 8c-d, s6a, s6c-d).

Overall, the incorporation of Apt02-tFNA into the DNA hydrogel endows it with dual functionalities: not only the capability for angiogenesis but also the tFNA-mediated enhancement of osteogenic differentiation. This multifaceted approach is poised to significantly amplify the ability of hydrogel to facilitate bone regeneration. The synergistic effect of Apt02-tFNA within the DNA hydrogel matrix presents a novel strategy for bone tissue engineering. While Apt02 drives the formation of new blood vessels, essential for providing nutrients and oxygen to the regenerating bone, tFNA concurrently stimulates the differentiation of osteoprogenitor cells into bone-forming cells. This dual action effectively addresses two critical aspects of bone healing - vascularization and osteogenesis - thereby potentially leading to more rapid and robust bone regeneration. The enhanced bone regenerative capacity offered by this hybrid system marks a significant advancement in the field and

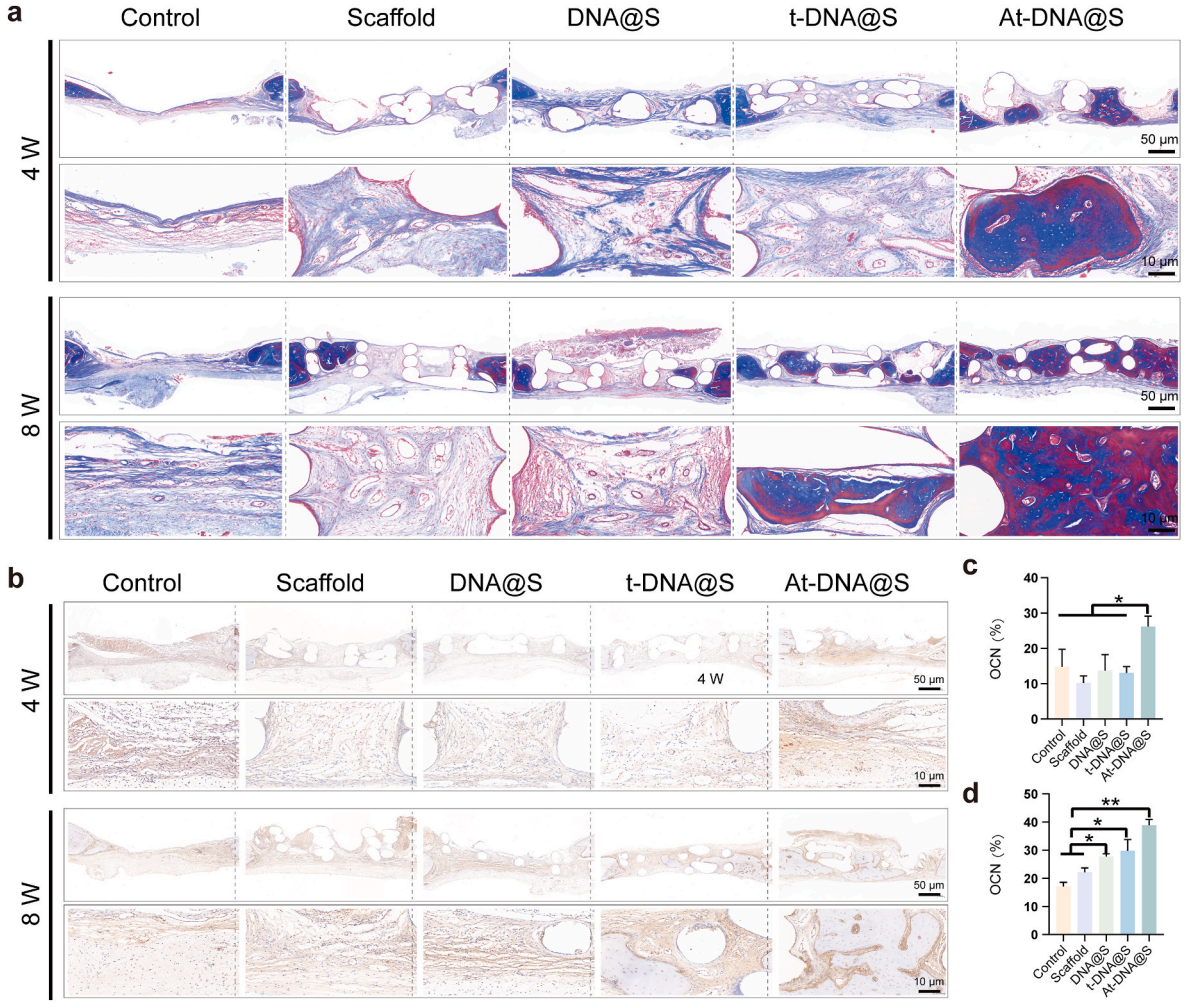

Fig. 7. Expression of matrix and marker proteins in the bone defect after gel-scaffold construct implantation. (a) Masson's trichrome staining images of cranial defects after the implantation of scaffold constructs for 4 and 8 weeks. (b) OCN immunohistochemical staining images of cranial defects after the implantation of scaffold constructs for 4 and 8 weeks. (c and d) Quantitative analysis of OCN immunohistochemical staining for 4 and 8 weeks. *p < 0.05, **p < 0.01, and ***p < 0.001.

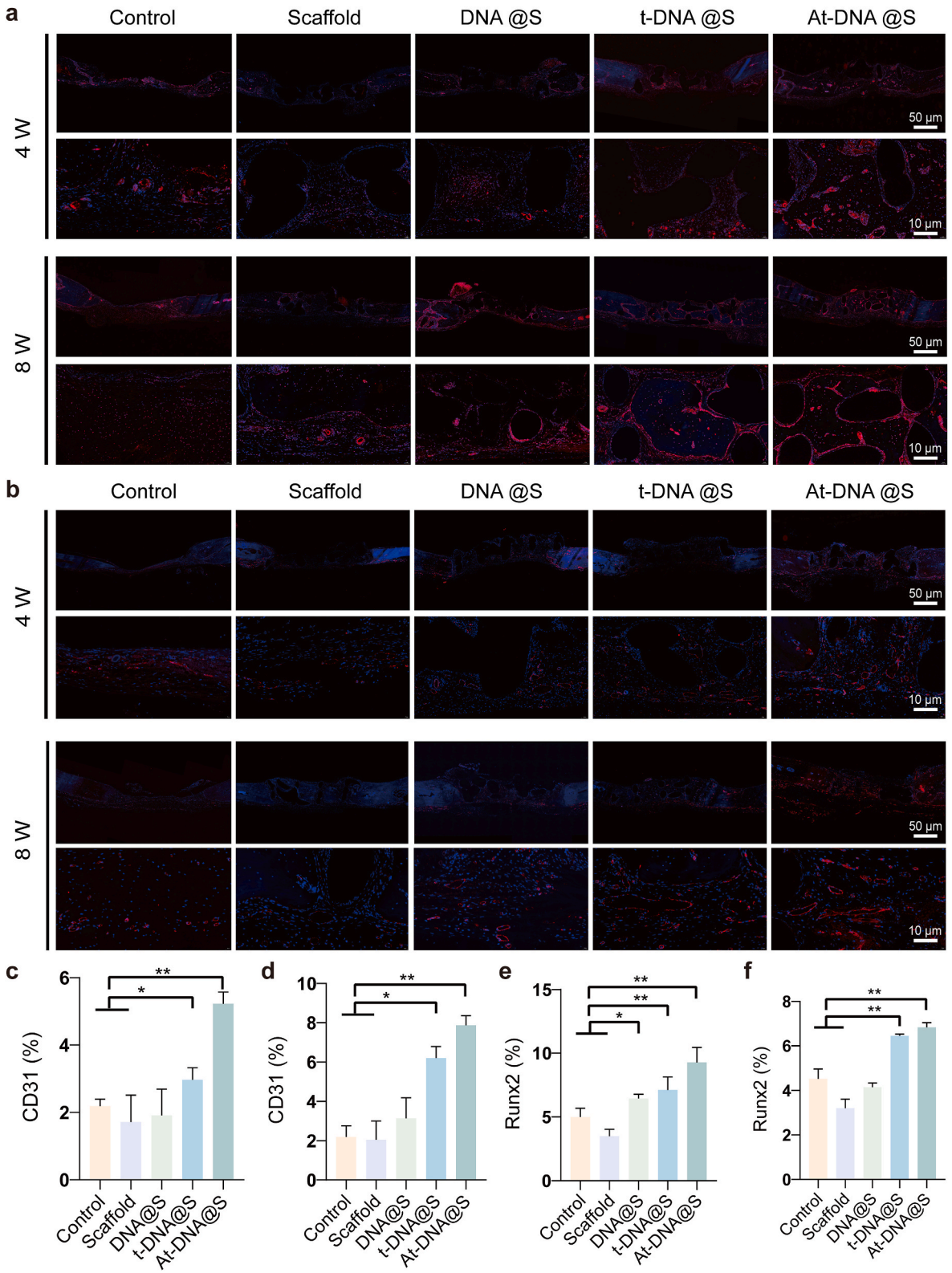

Fig. 8. Expression of immunofluorescence markers in bone defects after implantation of gel scaffolds. (a) CD31 immunofluorescence staining images of cranial defects after the implantation of scaffold constructs for 4 and 8 weeks. (b) RUNX2 immunofluorescence staining images of cranial defects after the implantation of scaffold constructs for 4 and 8 weeks. (c and d) Quantitative analysis of CD31 immunofluorescence staining for 4 and 8 weeks. (e and f) Quantitative analysis of RUNX2 immunofluorescence staining for 4 and 8 weeks. *$p < 0.05$, and **$p < 0.01$.

suggests promising applications in treating complex bone defects. The results from the cranial bone defect model prove the potential of At-DNA@S in treating bone defects and enhancing bone formation. This material, primarily synthesized from nucleic acid components, demonstrates excellent biocompatibility, offering a safe and effective biomaterial solution for future bone repair and challenging bone regeneration applications.

4. Conclusion

In conclusion, the At-tFNA@S group demonstrated significantly enhanced mineralization capabilities in bone regeneration. The DNA hydrogel component within this group exhibited excellent biocompatibility, low cost, and prolonged degradation time, making it well-suited for bone repair applications. The loaded Apt-tFNA in this formulation not only promotes bone formation but also facilitates rapid angiogenesis. This dual functionality endows the At-tFNA@S group with robust osteogenic capacity. The unique combination of these properties in the At-tFNA@S group underscores its potential as an effective material for bone tissue engineering, offering a promising approach for enhancing bone regeneration and repair.

CRediT authorship contribution statement

Yafei Han: Writing – original draft, Methodology, Investigation, Formal analysis, Data curation, Conceptualization. **Yan Wu:** Methodology, Funding acquisition, Data curation. **Fuxiao Wang:** Methodology, Investigation, Formal analysis, Data curation. **Guangfeng Li:** Project administration, Methodology, Data curation. **Jian Wang:** Supervision, Software. **Xiang Wu:** Visualization, Validation. **Anfu Deng:** Software. **Xiaoxiang Ren:** Methodology, Conceptualization. **Xiuhui Wang:** Supervision, Formal analysis. **Jie Gao:** Validation, Supervision, Conceptualization. **Zhongmin Shi:** Visualization, Validation. **Long Bai:** Writing – review & editing, Visualization, Conceptualization. **Jiacan Su:** Writing – review & editing, Supervision, Resources, Funding acquisition, Conceptualization.

Declaration of competing interest

The authors declare that they have no known competing financial interests or personal relationships that could have appeared to influence the work reported in this paper.

Acknowledgements

This work was financially supported by National Natural Science Foundation of China (82230071, 82172098), Integrated Project of Major Research Plan of National Natural Science Foundation of China (92249303), Shanghai Committee of Science and Technology (23141900600, Laboratory Animal Research Project), Shanghai Clinical Research Plan of SHDC2023CRT01.

Appendix A. Supplementary data

Supplementary data to this article can be found online at https://doi.org/10.1016/j.bioactmat.2024.01.009.

References

[1] S. Grässel, J. Lorenz, Tissue-engineering strategies to repair chondral and osteochondral tissue in osteoarthritis: use of mesenchymal stem cells, Curr. Rheumatol. Rep. 16 (2014) 452.
[2] H.C. Pape, A. Evans, P. Kobbe, Autologous bone graft: properties and techniques, J. Orthop. Trauma 24 (2010) S36–S40.
[3] L. Sun, Y.Y. Hu, Z.J. Ning, Z. Liang, The correlation between immune rejection and osteoinduction of allogeneic bone grafting, Chinese Med J 111 (1998) 818–822.
[4] L. Bai, Y. Wu, G. Li, W. Zhang, H. Zhang, J. Su, AI-enabled organoids: construction, analysis, and application, Bioact. Mater. 31 (2024) 525–548.
[5] Y. Lu, S. Deshmukh, I. Jones, Y.L. Chiu, Biodegradable magnesium alloys for orthopaedic applications, Biomaterials translational 2 (2021) 214–235.
[6] X. Xue, Y. Hu, S. Wang, X. Chen, Y. Jiang, J. Su, Fabrication of physical and chemical crosslinked hydrogels for bone tissue engineering, Bioact. Mater. 12 (2022) 327–339.
[7] E. Steijvers, A. Ghei, Z. Xia, Manufacturing artificial bone allografts: a perspective, Biomaterials translational 3 (2022) 65–80.
[8] J. Zhou, H. Lin, T. Fang, X. Li, W. Dai, T. Uemura, J. Dong, The repair of large segmental bone defects in the rabbit with vascularized tissue engineered bone, Biomaterials 31 (2010) 1171–1179.
[9] M. Wu, H. Liu, D. Li, Y. Zhu, P. Wu, Z. Chen, F. Chen, Y. Chen, Z. Deng, L. Cai, Smart-Responsive Multifunctional Therapeutic System for Improved Regenerative Microenvironment and Accelerated Bone Regeneration via Mild Photothermal Therapy, Advanced Science (Weinheim, Baden-Wurttemberg, Germany, 2023 e2304641.
[10] N. Amiryaghoubi, M. Fathi, N.N. Pesyan, M. Samiei, J. Barar, Y. Omidi, Bioactive polymeric scaffolds for osteogenic repair and bone regenerative medicine, Med. Res. Rev. 40 (2020) 1833–1870.
[11] M.P. Nikolova, M.S. Chavali, Recent advances in biomaterials for 3D scaffolds: a review, Bioact. Mater. 4 (2019) 271–292.
[12] J.O. Jin, G. Kim, J. Hwang, K.H. Han, M. Kwak, P.C.W. Lee, Nucleic acid nanotechnology for cancer treatment, Biochimica et biophysica acta, Reviews on cancer 1874 (2020) 188377.
[13] S. Sethi, H. Sugiyama, M. Endo, Biomimetic DNA nanotechnology to understand and control cellular responses, Chembiochem 23 (2022) e202100446.
[14] Y. Han, L. Cao, G. Li, F. Zhou, L. Bai, J. Su, Harnessing nucleic acids nanotechnology for bone/cartilage regeneration, Small 19 (2023) e2301996.
[15] Y. Shao, C. Li, X. Zhou, F. Wu, H. Jia, Y. Wang, D. Liu, Supramolecular DNA hydrogel, Polym. Bull. (2015) 100–108.
[16] D. Athanasiadou, N. Meshry, N.G. Monteiro, A.C. Ervolino-Silva, R.L. Chan, C. A. McCulloch, R. Okamoto, K.M.M. Carneiro, DNA hydrogels for bone regeneration, Proc. Natl. Acad. Sci. U. S. A. 120 (2023) e2220565120.
[17] T. Zhang, T. Tian, Y. Lin, Functionalizing framework nucleic-acid-based nanostructures for biomedical application, Adv. Mater. 34 (2022) e2107820.
[18] Y. Lin, Q. Li, L. Wang, Q. Guo, S. Liu, S. Zhu, Y. Sun, Y. Fan, Y. Sun, H. Li, X. Tian, D. Luo, S. Shi, Advances in regenerative medicine applications of tetrahedral framework nucleic acid-based nanomaterials: an expert consensus recommendation, Int. J. Oral Sci. 14 (2022) 51.
[19] W. Ma, Y. Zhan, Y. Zhang, X. Xie, C. Mao, Y. Lin, Enhanced neural regeneration with a concomitant treatment of framework nucleic acid and stem cells in spinal cord injury, ACS Appl. Mater. Interfaces 12 (2020) 2095–2106.
[20] S.M. Chim, J. Tickner, S.T. Chow, V. Kuek, B. Guo, G. Zhang, V. Rosen, W. Erber, J. Xu, Angiogenic factors in bone local environment, Cytokine Growth Factor Rev. 24 (2013) 297–310.
[21] M. Wu, F. Chen, P. Wu, Z. Yang, S. Zhang, L. Xiao, Z. Deng, C. Zhang, Y. Chen, L. Cai, Bioinspired redwood-like scaffolds coordinated by in situ-generated silica-containing hybrid nanocoatings promote angiogenesis and osteogenesis both in vitro and in vivo, Adv. Healthcare Mater. 10 (2021) e2101591.
[22] H. Liu, F. Chen, Y. Zhang, P. Wu, Z. Yang, S. Zhang, L. Xiao, Z. Deng, L. Cai, M.J. M. Wu, Design, Facile fabrication of biomimetic silicified gelatin scaffolds for angiogenesis and bone regeneration by a bioinspired polymer-induced liquid precursor, Mater. Des. 222 (2022) 111070.
[23] D. Zhao, M. Liu, J. Li, D. Xiao, S. Peng, Q. He, Y. Sun, Q. Li, Y. Lin, Angiogenic aptamer-modified tetrahedral framework nucleic acid promotes angiogenesis in vitro and in vivo, ACS Appl. Mater. Interfaces 13 (2021) 29439–29449.
[24] S. Li, Y. Liu, T. Tian, T. Zhang, S. Lin, M. Zhou, X. Zhang, Y. Lin, X. Cai, Bioswitchable delivery of microRNA by framework nucleic acids: application to bone regeneration, Small 17 (2021) e2104359.
[25] A. Sadeghi, S.M.A. Razavi, D. Shahrampour, Fabrication and characterization of biodegradable active films with modified morphology based on polycaprolactone-polylactic acid-green tea extract, Int. J. Biol. Macromol. 205 (2022) 341–356.
[26] J.A. Elias, R.J. Zitnik, Cytokine-cytokine interactions in the context of cytokine networking, Am. J. Respir. Cell Mol. Biol. 7 (1992) 365–367.
[27] N.-G. Kim, E. Koh, X. Chen, B.M. Gumbiner, E-cadherin mediates contact inhibition of proliferation through Hippo signaling-pathway components, P. NATL. ACAD. SCI. USA. 108 (2011) 11930–11935.
[28] J.B. Huang, S. Wu, J. Barrera, K. Matthews, D.J. Pan, The Hippo signaling pathway coordinately regulates cell proliferation and apoptosis by inactivating Yorkie, the *Drosophila* homolog of YAP, Cell 122 (2005) 421–434.
[29] K. Hu, B.R. Olsen, Osteoblast-derived VEGF regulates osteoblast differentiation and bone formation during bone repair, J. Clin. Invest. 126 (2016) 509–526.
[30] Y. Li, C. Huang, A. Duan, M. Li, X. Zhang, L. Lu, L. Yu, L. Yu, P. Liu, K. Chen, Y. Jiang, A temperature-sensitive DNA-PNIPAAm hydrogel prepared by base pairing, Colloid Polym. Sci. 301 (2023) 383–388.
[31] J. Gačanin, A. Kovtun, S. Fischer, V. Schwager, J. Quambusch, S.L. Kuan, W. Liu, F. Boldt, C. Li, Z. Yang, D. Liu, Y. Wu, T. Weil, H. Barth, A. Ignatius, Spatiotemporally controlled release of rho-inhibiting C3 toxin from a protein-DNA hybrid hydrogel for targeted inhibition of osteoclast formation and activity, Adv. Healthcare Mater. 6 (2017) 1700392.
[32] X. Shao, S. Lin, Q. Peng, S. Shi, X. Wei, T. Zhang, Y. Lin, Tetrahedral DNA nanostructure: a potential promoter for cartilage tissue regeneration via regulating chondrocyte phenotype and proliferation, Small 13 (2017) 1602770.
[33] S. Gan, Z. Zheng, M. Zhang, L. Long, X. Zhang, B. Tan, Z. Zhu, J. Liao, W. Chen, Lyophilized platelet-rich fibrin exudate-loaded carboxymethyl chitosan/GelMA hydrogel for efficient bone defect repair, ACS Appl. Mater. Interfaces 15 (2023) 26349–26362.

[34] S. Gan, Y. Wu, X. Zhang, Z. Zheng, M. Zhang, L. Long, J. Liao, W. Chen, Recent advances in hydrogel-based phototherapy for tumor treatment, Gels (Basel, Switzerland) 9 (2023) 286.
[35] A. Lex, N. Gehlenborg, H. Strobelt, R. Vuillemot, H. Pfister, UpSet: visualization of intersecting sets, IEEE Trans. Vis. Comput. Graph. 20 (2014) 1983–1992.
[36] S. Piccolo, S. Dupont, M. Cordenonsi, The biology of yap/taz: HIPPO signaling and beyond, Physiol. Rev. 94 (2014) 1287–1312.
[37] S. Boonrungsiman, E. Gentleman, R. Carzaniga, N.D. Evans, D.W. McComb, A. E. Porter, M.M. Stevens, The role of intracellular calcium phosphate in osteoblast-mediated bone apatite formation, P. NATL. ACAD. SCI. USA. 109 (2012) 14170–14175.
[38] H. Li, T. Li, J. Fan, T. Li, L. Fan, S. Wang, X. Weng, Q. Han, R.C. Zhao, miR-216a rescues dexamethasone suppression of osteogenesis, promotes osteoblast differentiation and enhances bone formation, by regulating c-Cbl-mediated PI3K/AKT pathway, Cell Death Differ. 22 (2015) 1935–1945.
[39] P.A. Beachy, S.S. Karhadkar, D.M. Berman, Tissue repair and stem cell renewal in carcinogenesis, Nature 432 (2004) 324–331.
[40] K.D. Hankenson, K. Gagne, M. Shaughnessy, Extracellular signaling molecules to promote fracture healing and bone regeneration, Adv. Drug Deliv. Rev. 94 (2015) 3–12.
[41] H. Liu, G.W. Xu, Y.F. Wang, H.S. Zhao, S. Xiong, Y. Wu, B.C. Heng, C.R. An, G. H. Zhu, D.H. Xie, Composite scaffolds of nano-hydroxyapatite and silk fibroin enhance mesenchymal stem cell-based bone regeneration via the interleukin 1 alpha autocrine/paracrine signaling loop, Biomaterials 49 (2015) 103–112.